Journal of Applied Fluid Mechanics, Vol. 14, No. 5, pp. 1583-1591, 2021.
Available online at www.jafmonline.net, ISSN 1735-3572, EISSN 1735-3645.
https://doi.org/10.47176/jafm.14.05.32343

Numerical Research on Effect of Base Bleed Type on Operation Process of Base Bleed Projectile

M. Wang and C. Zhuo†

School of Mechanical Engineering, Nanjing University of Science and Technology, Nanjing, Jiangsu, 210094, China

†*Corresponding Author Email: njust203zcf@126.com*

(Received November 3, 2020; accepted April 6, 2021)

ABSTRACT

The edge base bleed type is presented in this paper. Based on the advantages of computational fluid dynamics and the firing range prediction of base bleed projectile, the flight ballistic of base bleed projectile with two kinds of base bleed type is solved by using the computational aerodynamics coupled with particle trajectory, obtained the change laws of operation parameter, flow filed of base bleed projectile with time. The results show that: The performance of the edge base bleed type is better than that of the traditional center base bleed type, and the fire range of the base bleed projectile with edge type is about 2 km higher than that of the center type. The base bleed parameter of the two kinds of base bleed type at the state of drag reduction increase first and then decrease with the increase of time. For the center base bleed type, the drag coefficient increases with time. For the edge base bleed type, the drag coefficient is nearly stable at the reduction state, and is always smaller than that of the center base bleed type. The base flow structure of the edge base bleed type does not change with both the time and base bleed parameter. The base bleed gas always forms the main recirculation zone at the bottom of projectile and plays the role of drag reduction.

Keywords: Computational fluid dynamics; Base bleed projectile; Base bleed type; Firing range.

1. INTRODUCTION

One of the ways to reduce base drag of projectiles is concept of base bleed. The principle is to append a base bleed unit filled with propellant to the bottom of conventional projectiles, as schematically shown in Fig. 1. The base bleed unit injects gas with a low velocity and high temperature into the base recirculation zone increasing the base pressure and subsequently reducing base drag. The base bleed projectile has been intensively investigated both experimentally and numerically during the past years (Guo 1994; Ding *et al.* 2000, 2002; Zhuo *et al.* 2014a ,b and 2015; Mathur and Dutton 1996; Choi 2005; Luo *et al.* 2015).

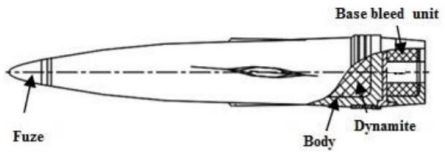

Fig. 1. Schematic of base bleed projectile.

For instance, Ding *et al.* (2000,2002) develops wind tunnel test on base bleed drag reduction to obtain drag reduction mechanism. Zhuo *et al.* (2014a ,b) conducts the study of drag reduction mechanism and characteristics under the condition of real base bleed gas. Based on the method of coupling CFD and particle trajectory, the operation process of the base bleed projectile is solved, and the effecting laws of burning rate of propellant and altitude on operation characteristics of the base bleed projectile is studied by Zhuo *et al.* (2015). Mathur and Dutton(1996) performs a wind tunnel test using cold base bleed gas to study the drag reduction mechanism. Choi (2005) simulates the two-dimensional axisymmetric flow field of the 155mm projectile by adopting the k-ω turbulent flow model and the laminar combustion finite rate elementary reaction model. Ma and Yu (2019) uses a semi-closed bomb to simulate the rapid depressurization process during the ejection of base bleed projectile from the muzzle, and studied the combustion gas flow characteristics of propellant and the transient combustion characteristics of igniter. Through adopting the improved advection upstream splitting method scheme and the shear stress transport k-ω turbulence model, the effects of different nozzle structures on the wake flow field characteristics of base-bleed projectile under transient depressurization are investigated by Zhou and Yu (2020). Zhang *et al.* (2018) researches the drag reduction characteristics of the 155 mm base

bleed projectile and reduces the range dispersion of a base bleed projectile by establishing the initial propellant temperature modified model, interior ballistic model and exterior ballistic model. The burning models for base bleed propellant with different burning rate, cladding layer position were established to research the drag reduction and extend range characteristics of base bleed projectile by Zhang and Zhang (2017).

At present the base exhaust mode of the base bleed projectile is central type, and the high temperature gas flow from the center hole of the projectile bottom to the wake flow field. If the high temperature gas discharge from the edge of projectile bottom to the wake flow field, how will this affect the drag reduction performance compared to the conventional central type? The two kinds of exhaust structures are shown in Fig. 2.

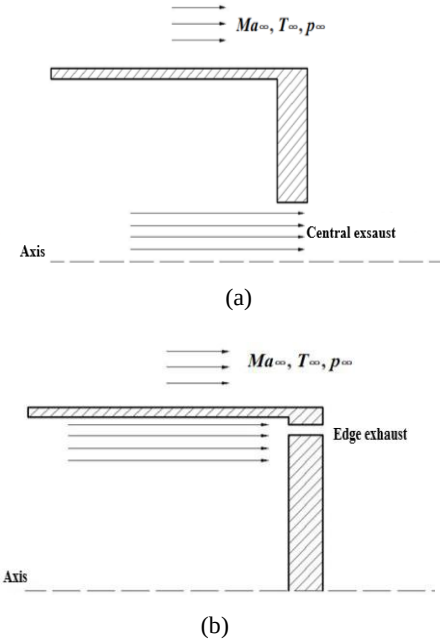

Fig. 2. Schematic of the two base bleed types, (a) central type, (b) edge type.

Based on the calculation model of the operation process of the base bleed projectile coupling CFD and particle trajectory in Zhuo *et al*. (2015), this paper obtains the changes in the operation parameters, operation state, and the flow field of the two kinds of exhaust structure in the stage of drag reduction, as well as the influence of the exhaust structure on the drag reduction performance and the increase efficiency of firing range. This work can provide an important reference for the research on base bleed projectile and drag reduction.

2. MATHEMATICS METHOD AND PHYSICAL MODEL

2.1 Mathematics Method

Assuming that the flow in this present study is two-dimensional axisymmetric ignoring both the attack angle, and the time-dependent Navier-Stokes equations with chemical non-equilibrium are expressed in the integral form as Ouyang *et al*. (2001):

$$\frac{\partial U}{\partial t}+\frac{\partial F}{\partial x}+\frac{\partial G}{\partial y}=\frac{\partial F_v}{\partial x}+\frac{\partial G_v}{\partial y}+H+S \tag{1}$$

where U is the vector of the conservative variables, F, G are the vector of the convective flux, F_v, G_v are the vector of the viscosity flux, S is the vector of source term caused by chemical reactions, H is the vector of source term caused by axial symmetry.

The k-w SST turbulence model (Menter 1994) is used in this paper, which plays a good performance in separation flow. Taking the strong turbulence in the combustion chamber into account, the turbulence combustion model based on the second-order moment (Zhuo 2002) is used to describe the interaction between the chemical reaction and turbulence flow.

The convective flux is solved by using AUSMPW+ scheme (Kim 1998), and time integration is performed by using the third-order total variation diminishing Runge-Kutta method. The viscous term is discretized in the central scheme, and single step method is used for time discretion, and the region time steps method is used to accelerate the convergence. The form of turbulence equations is consistent with the Navier-Stokes equations, so it can be coupled with the Navier-Stokes equations, and then solved.

In the chemical reaction flow, the characteristic chemical time (τ_{chem}) is much smaller than the characteristic flow time(τ_{flow}), meaning the Damkohler number (Da= τ_{flow}/τ_{chem}) is much larger than 1, and then the stiff problem is formed.

The governing equations of chemical non-equilibrium flow are divided into flow part and chemical reactions part, which mutually couple and produce stiffness problem. The time-operator splitting algorithm is used to deal with the stiff problem. This is accomplished by first freezing the chemical reaction to solve the flow field and obtain parameters, and then regarding the chemical reaction as an equal volume exothermic or endothermic process, to make the internal energy and velocity parameters remain constant, at the same time calculating the mass-change rate of each component. Finally, the temperature and other parameters of the flow field are obtained by iteration computation.

One of the keys to determine the success of the chemical non-equilibrium flow simulation is the chemical reaction kinetic model. In the current work, the chemical reaction kinetic model of carbon monoxide oxidation involves eight species (CO, H_2, O_2, CO_2, H_2O, H, OH, O), one inert specie (N_2) and twelve elementally reactions steps (Choi 2005), which are shown in Table. 1.

The detailed description and verification of calculation methods in the CFD program that are developed by our research group are shown in Zhuo *et al.* (2014a ,b), which will not be repeated here.

Table 1 Chemical reaction kinetic model of CO-H_2-O_2 system.

Detailed reaction	A	b	E
$H+O_2 \leftrightarrow OH+O$	1.2×10^{17}	-0.91	69.1
$H_2+O \leftrightarrow OH+H$	1.5×10^{7}	2.0	31.6
$O+H+M \leftrightarrow OH+M$	1.0×10^{16}	0.0	0.0
$O+O+M \leftrightarrow O_2+M$	1.0×10^{17}	-1.0	0.0
$H+H+M \leftrightarrow H_2+M$	9.7×10^{16}	-0.6	0.0
$H_2O+M \leftrightarrow H+OH+M$	1.6×10^{17}	0.0	478.0
$O+H_2O \leftrightarrow OH+OH$	1.5×10^{10}	1.14	72.2
$OH+H_2 \leftrightarrow H_2O+H$	1.0×10^{8}	1.6	13.8
$H_2+O_2 \leftrightarrow OH+OH$	7.94×10^{14}	0.0	187.0
$CO+OH \leftrightarrow CO_2+H$	4.4×10^{6}	1.5	-3.1
$CO+O+M \leftrightarrow CO_2+M$	5.3×10^{13}	0.0	-19.0
$CO+O_2 \leftrightarrow CO_2+O$	2.5×10^{12}	0.0	200.0

The Arrhenius form is $K_f = AT^b \exp(-E / R_0 / T)$; the units of factor A is $[cm^3/mol]^{n-1}sec^{-1}$, where n is the chemical reaction progression; b is the temperature index, E is the activation energy, R_0 is the specific gas constant; M represents the third body collision.

2.2 The Particle Trajectory Model

The particle trajectory model mainly assumes that the attack angle of the projectile is zero during the flight and the projectile is an axisymmetric body, which makes the air drag and the gravity act on the mass center of projectile. Therefore, the motion of projectile can be treated as a particle trajectory model.

Because of the large amount of computation in CFD, it is impossible to use CFD to calculate the flow field in real time and provide the drag coefficient for the particle ballistic equations. In this paper, a loosely coupled method is used to solve the solution of particle ballistic equations and CFD, that is, after the particle trajectory equation is solved forward by the k step, and then CFD is used to calculate the drag coefficient of projectile. This calculation process repeats until the projectile fall to the ground. As the propelling time step of particle ballistic equation is 0.001s, it is advisable to use k=500, that is, after every movement of 0.5s, the flow field and drag coefficient of the base bleed projectile at this position are calculated by CFD. As the flight velocity, environmental pressure and environmental density vary little in each time period of 0.5s, the drag coefficient is considered as a constant in this period. Therefore, this loosely coupled processing method is reasonable (Zhuo *et al.* 2015).

2.3 Physical Model

In this paper, a typical base bleed projectile is taken as the research object. The relative dimensions of the projectile are shown in Fig. 3. And the calculation

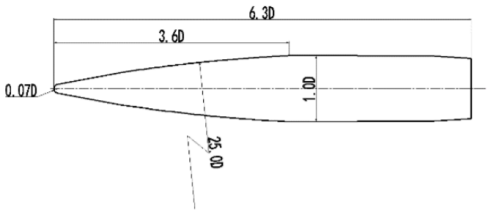

Fig. 3. Main geometry of the projectile (D is diameter of the projectile).

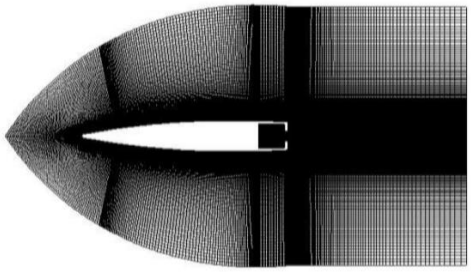

(a)

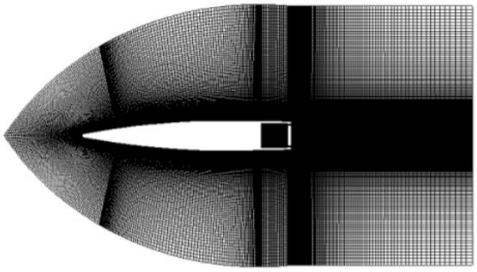

(b)

Fig. 4. Computation grid of base bleed projectile, (a) Central type, (b) Edge type.

grid corresponding to the two kinds of exhaust structure is shown in Fig. 4 and the exhaust area of two kinds of exhaust structure is the same which is both 1778.5 mm^2. Since the computational domain is two-dimensional axisymmetric model, only the upper half plane flow filed need to be calculated. In order to observation, the flow field data of the lower half plane are obtained based on symmetry. In the flight, both the combustion area of base bleed propellant and the volume of combustion chamber are constantly changing, and the shape of the propellant is complex, so it cannot be simplified as a two-dimensional axisymmetric model. Therefore, in this paper the combustion chamber and the propellant shape are fixed. It is assumed that one surface in combustion chamber is the burning surface of the propellant, and the mass flow rate of the propellant combustion, which is coupled with the change law of the burning surface and the calculation of the flow field, is applied on the assumed combustion surface.

The mass of the projectile before launching is 31.8 kg, and the initial velocity of launching is 947 m/s.

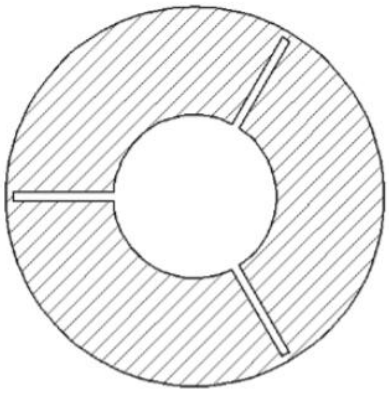

Fig. 5. Cross section of base bleed propellant.

The projectile is launched at an angle of 52 degrees. The base bleed propellant is three petal structure, and both ends and the outer side are covered by a thermal insulation layer. The cross section of the propellant is shown in Fig. 5. The external diameter of the propellant is 100 mm, the inner diameter is 44 mm, the length is 97 mm, and the slit width is 2 mm. The density of the propellant is 1520 kg/m^3, the burning temperature of the propellant is 1812 K, and the burning law obeys the geometric combustion law.

The formula for burning rate of propellant:

$$\dot{r} = \varepsilon a p^n \tag{2}$$

where the burning rate correction coefficient ε =1.3 is the correction factor of burning rate caused by the projectile rotation. The burning rate coefficient a is 4.903×10^{-6}, and the unit is m/(s·Pa^n). p is the pressure in combustion chamber, and the unit is Pascal (Pa). n = 0.484 is the burning pressure index of the propellant. The parameters mentioned above are constant and obtained by experiments.

The mass flow rate of base bleed gas generated by the propellant can be calculated by the combustion area, burning rate and the density of propellant, which can be used as the boundary condition of the burning surface in CFD. However, the burning rate of propellant is related to the pressure of the flow field. The mass flow rate of base bleed gas applied to the burning surface boundary is as follow:

$$\dot{m} = \rho_s \dot{r} S = \rho_s \varepsilon a p^n S \tag{3}$$

This mass flow rate also affects the combustion chamber pressure in the CFD calculation. Therefore, in the calculation of the flow field at a certain time, the calculation of CFD flow field and the mass flow rate of base bleed gas need to be coupled with each other until the flow field reaches stability.

3. NUMERICAL RESULTS AND DISCUSSION

In table. 2, the operation parameters of the two types of base bleed projectiles, including the time of propellant combustion, the time of flight, firing range and the increase rate of firing range, are given. It can

Table 2 Operating parameters of base bleed projectile for two base bleed types.

Operating parameter	central type	edge type
The time of propellant combustion, s	25	23
The time of flight, s	114	119
Firing range X, km	36.8	38.9
The increase rate of firing range δ	29.4%	34.7%

be seen from the table that for the central type the firing range is 36.8 km, the flight time is 114 s, and the increase rate of firing range is 29.4 % compared with the standard firing range of 28.5 km of the ordinary projectile without the base bleed. The propellant combustion time of the edge type is slightly less than that of the central type. The firing range of the edge type increase about 2 km compared with that of the central type, and the increase rate of firing range increase from 29.4% to 34.7%. These results show that the drag reduction performance of the base bleed projectile with the edge type is superior to the base bleed projectile with the central type.

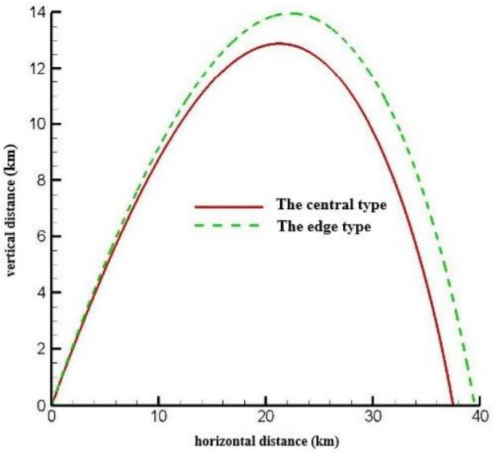

Fig. 6. Flight trajectory of the projectile for two base bleed types.

Figure 6 shows the flight trajectories of two kinds of base bleed projectile. In the drag reduction stage, the ballistics of the two kinds of projectile is basically identical. After the horizontal displacement of 10 km, there is obvious difference in the two kinds of flight trajectory. Figure 7 and Fig. 8 shows the variation of horizontal displacement and vertical displacement of two kind of projectile with time. Within 0~20s, the horizontal displacement of the two kind of projectile is basically identical, as well as the vertical displacement. This is due to the small difference in drag coefficient, and the time of this stage is short. It is not obvious that there is a difference in flight velocity. As a result, the horizontal displacement of the two kinds of projectile basically coincide, as well as the vertical

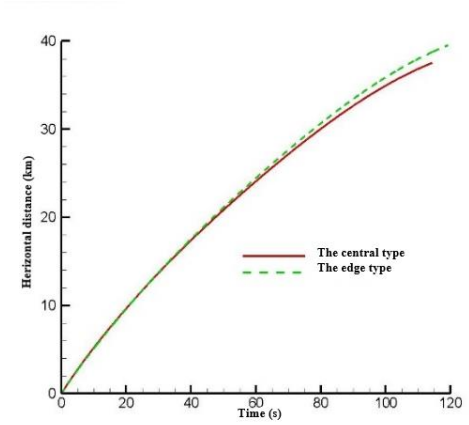

Fig. 7. Horizontal displacement of the base bleed projectile variation with time.

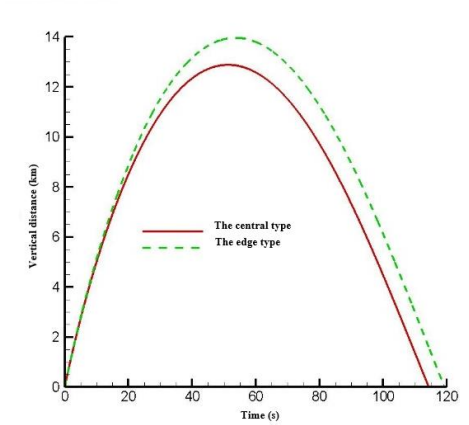

Fig. 8. Vertical displacement of base bleed projectile variation.

displacement. After 20 s, the horizontal displacement of two kinds of projectile has obvious difference with time as well as the vertical displacement. And with the increase of time, the difference also increases obviously. This is due to the difference in both the drag coefficient and the inflow air parameter.

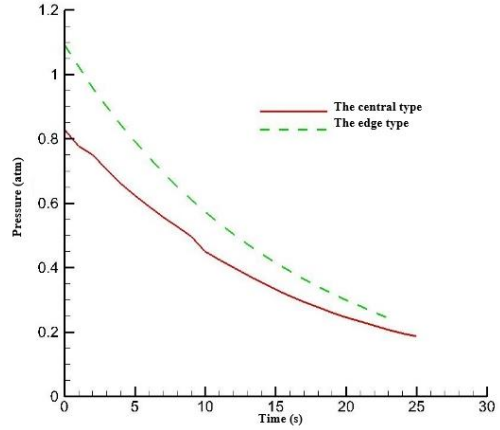

Fig. 9. Average pressure of combustion chamber at reduction stage variation with time.

Figure 9 shows the average pressure in the base bleed unit of the two kinds of projectile with time. In the process of drag reduction, the difference of the two kinds of base bleed structures leads to the slightly difference of the process that the combustion chamber gas ejects in the environment, which causes the average pressure in the combustion chamber of the edge type always be higher than that of the central type during the drag reduction stage.

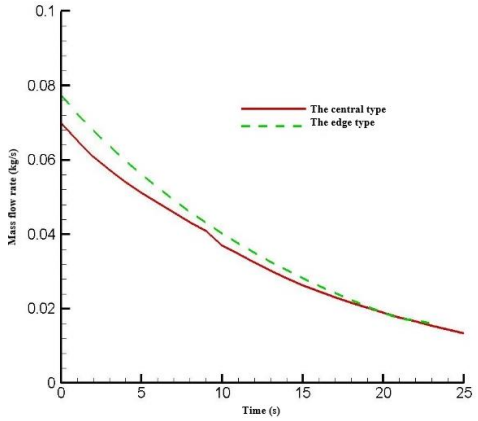

Fig. 10. Mass flow rate of base bleed at reduction stage variation with time.

Figure 10 shows the variation of the base bleed mass flow rate of two kinds of exhaust structure with time in drag reduction stage. According to the burning rate formula of the propellant, the higher the average pressure of the combustion chamber, the higher the burning rate are, as well as the gas generation under the same burning area. Therefore, from the law of change, the variation of the exhaust mass flow rate of two kinds of exhaust structure with time is basically the same with the variation of the combustion chamber pressure with time. In fact, the average pressure in combustion chamber is coupled with the exhaust mass flow rate. The higher average pressure of the combustion chamber leads to higher exhaust mass flow rate. When the exhaust mass flow rate is larger, the average pressure in the combustion chamber is higher under the same exhaust area.

Figure 11 shows the variation of the exhaust parameter of the two kinds of exhaust structure with time in drag reduction stage. The exhaust parameter I directly affects the exhaust drag reduction effect, which indicates the ratio of the exhaust mass flow rate to the facing air mass flow rate of projectile, and the mathematical definition formula is as follows:

$$I = \frac{\dot{m}}{\rho_{\inf} u_{\inf} S_{\text{ref}}} \tag{4}$$

Where $\rho_{\inf}$ is the density of the inflow air, $u_{\inf}$ is the velocity of the inflow air.

As can be seen in Fig. 11, exhaust parameter of base bleed projectile for different exhaust structures in the

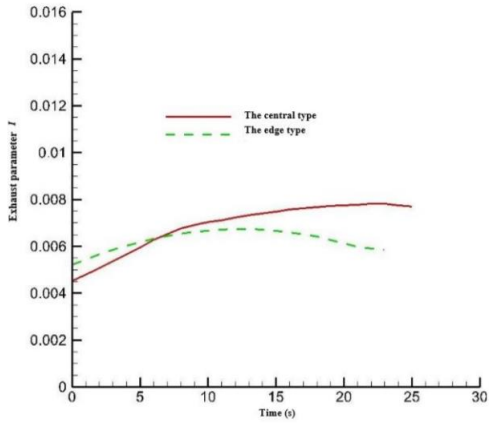

Fig. 11. Exhaust parameter of base bleed I at reduction stage variation with time.

drag reduction stage increases first and then decrease with time. In the initial stage of drag reduction, the gas exhaust flow rate decreases gradually with the time, while the windward air mass flow rate of the projectile gradually reduces, and the reduction degree is more violent than the gas exhaust mass flow rate. Therefore, the exhaust parameter increases with the time. But in the later stage of drag reduction, the exhaust parameter decreases with time. In the initial stage of drag reduction, the flow parameters of the two kinds of exhaust structure are basically identical, because the amount of the gas generated by the edge type of exhaust structure is large and the exhaust parameter of the edge type is higher than that of the central type. In the later stage of drag reduction, the gas exhaust flow rate decreases, but due to the difference in the drag in the early drag reduction stage, that is to say, the difference of inflow air parameter makes the exhaust parameter of the edge type exhaust structure is lower than that of the central type exhaust structure.

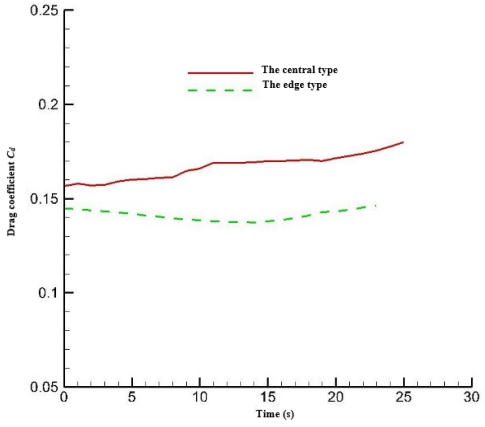

Fig. 12. Drag coefficient Cd at reduction stage variation with time.

Figure 12 shows the drag coefficient of the two kinds of exhaust structure changing with time during drag reduction. In the drag reduction stage, the Mach number of flight decreases with time. If there is no base bleed to reduce drag, the drag coefficient will increase with time according to the law of aerodynamics. As can be seen from Fig. 12, the drag coefficient of the central type of exhaust structure increase with time, while the drag coefficient of the edge type of exhaust structure is basically stable with time, and is always less than the central type exhaust structure. It is precisely because in the stage of drag reduction, the drag coefficient of edge type exhaust structure is always less than the central type exhaust structure, so the firing range of the base bleed projectile with the edge type is increased by about 2 km relative to the base bleed projectile with the central type.

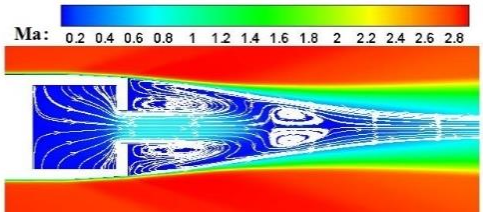

(a) t=0s

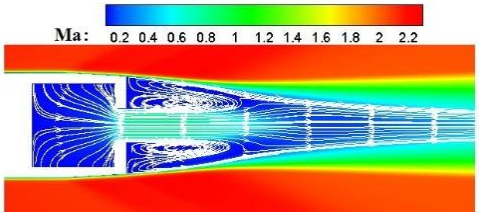

(b) t=10s

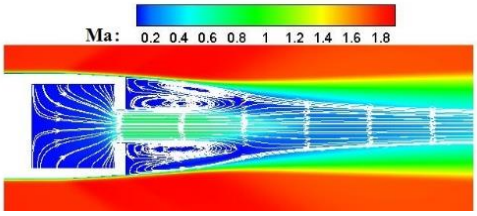

(c) t=20s

Fig. 13. Contours of Mach number and streamline in the bottom of the base bleed projectile with the central type.

Figure 13~Fig. 15 show the flow field contours of the base bleed projectile with the central type at the main time during the drag reduction stage. At the time of t=0s, both the exhaust parameter and the momentum of base bleed gas jet are small. The base bleed gas not only forms the main recirculation region with the inflow air on the central axis of the base tail flow field, but also forms the second recirculation region near the bottom of projectile with the inflow air. At the time of t=10s and t=20s, both the exhaust parameter and the momentum of base bleed gas jet are large. The bas bleed gas enters the wake directly

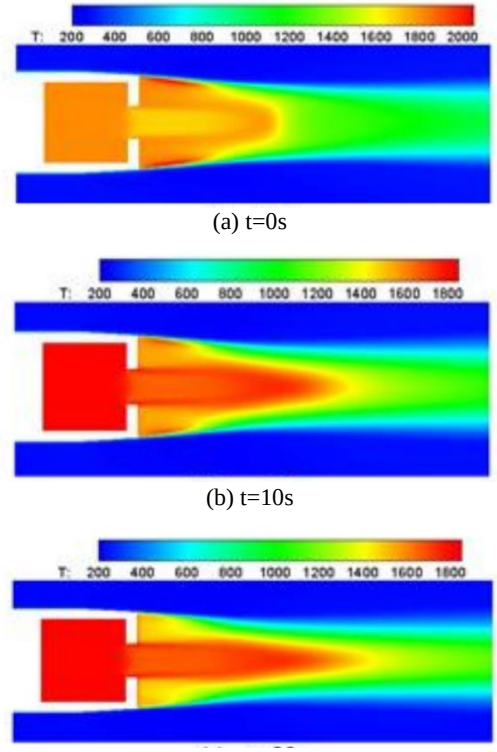

(a) t=0s

(b) t=10s

(c) t=20s

Fig. 14. Contours of temperature in the bottom of the base bleed projectile with the central type.

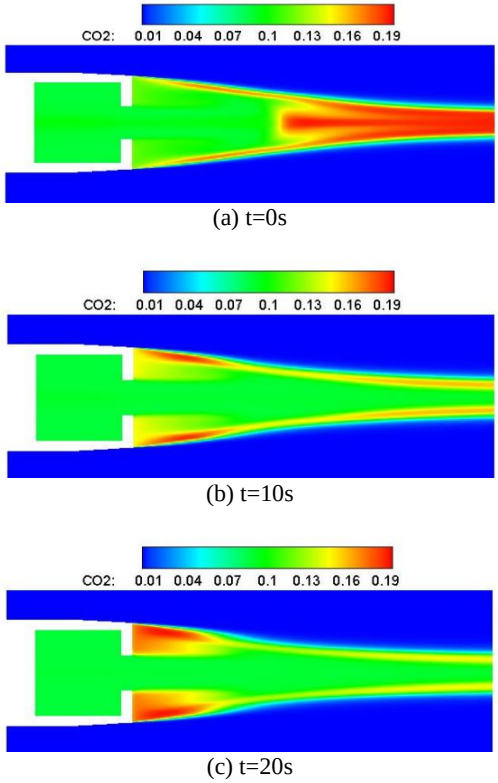

(a) t=0s

(b) t=10s

(c) t=20s

Fig. 15. Contours of CO_2 mass fraction in the bottom of the base bleed projectile with the central type.

in the form of jet, and does not form the main recirculation region with the inflow air on the axis. Since the base bleed flow filed of central type has been analyzed in detail in reference (Zhuo *et al.* 2014a ,b; 2015), there will be no more detail here.

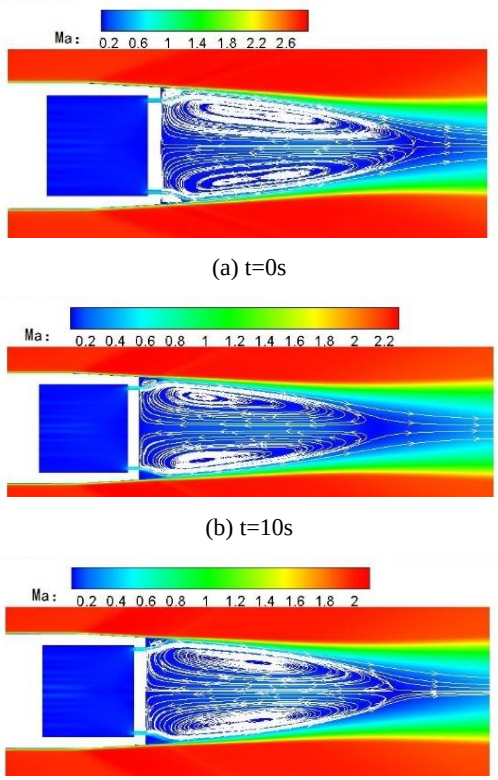

(a) t=0s

(b) t=10s

(c) t=20s

Fig. 16. Contours of Mach number and streamline in the bottom of the base bleed projectile with the edge type.

Figure 16~Fig. 18 show the flow field contours of the base bleed projectile with the edge type at the main time during the drag reduction stage. At the three main moments, the flow structure at the bottom is basically identical. After the base bleed gas is discharged from the edge, most of the base bleed gas will form the recirculation region at the bottom of the projectile and mix with the air. The difference between the flow field of the two kinds of exhaust structures is compared, which explains the reasons for the difference of drag coefficient between the edge type and the central type in Fig. 12. For the central type, the main recirculation region is formed in the wake flow when the exhaust parameter is small, and the base bleed gas burst directly to the far field when the exhaust parameter is large, that the base bleed gas does not fill the bottom effectively, and the drag reduction effect is not fully played. For the edge type, the exhaust parameter does not affect the structure of the bottom flow, and the base bleed gas will form the main recirculation region at the bottom of the projectile, which fill the bottom and play a drag reduction effect.

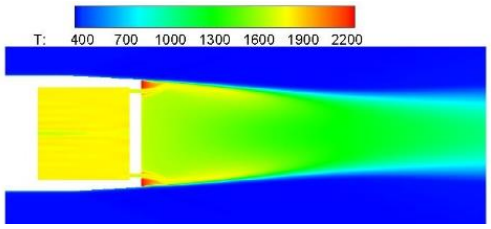

(a) t=0s

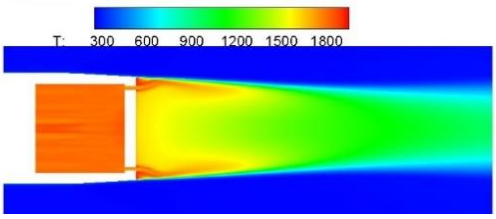

(b) t=10s

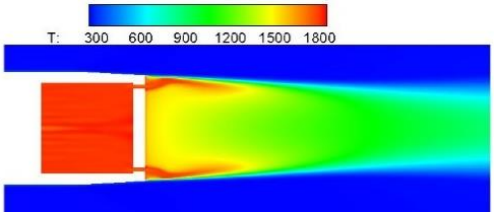

(c) t=20s

Fig. 17. Contours of temperature in the bottom of the base bleed projectile with the edge type.

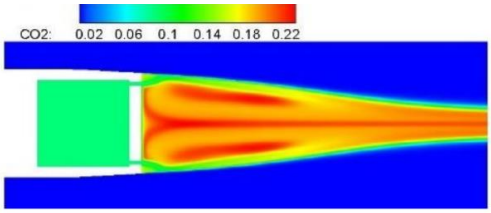

(a) t=0s

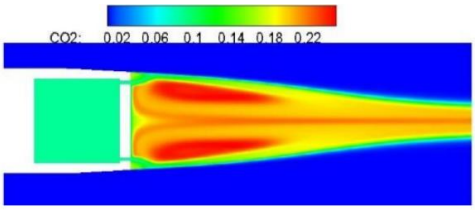

(b) t=10s

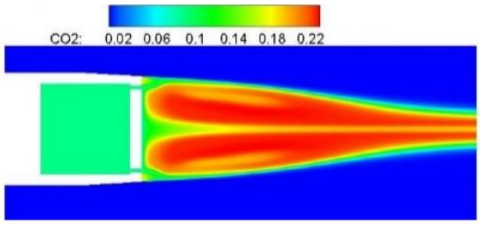

(c) t=20s

Fig. 18. Contours of CO_2 mass fraction in the bottom of the base bleed projectile with the edge type.

4. CONCLUSION

The firing range of the edge type increase about 2 km compared with that of the central type, and the increase rate of firing range increase from 29.4% to 34.7%. These results show that the drag reduction performance of the base bleed projectile with the edge type is superior to the base bleed projectile with the central type.

Exhaust parameters of base bleed projectile with different exhaust structures in the drag reduction stage increase first and then decrease with time. In the initial stage of drag reduction, the flow parameters of the two kinds of exhaust structure are basically identical. In the later stage of drag reduction, the exhaust parameter of the edge type exhaust structure is lower than that of the central type exhaust structure.

The drag coefficient of central type of exhaust structure increase with time, while the drag coefficient of edge type of exhaust structure is basically stable with time, and is always less than the central type exhaust structure. As a result, the firing range of the base bleed projectile with the edge type is increased by about 2 km relative to the base bleed projectile with the central type.

For the central type, the main recirculation region is formed in the wake flow when the exhaust parameter is small, and the base bleed gas burst directly to the far field when the exhaust parameter is large, that the base bleed gas does not fill the bottom effectively, and the drag reduction effect is not fully played. For the edge type, the exhaust parameter does not affect the structure of the bottom flow, and the base bleed gas will form the main recirculation region at the bottom of the projectile, which fill the bottom and play a drag reduction effect. So under the corresponding condition, the drag coefficient of the base bleed projectile with the edge type is always less than that of the base bleed projectile with the central type.

ACKNOWLEDGE

The study has been financially supported by the National Natural Science Foundation of China (No. 11802134), Jiangsu Provincial Natural Science Foundation, China (No. BK20180453) and China Postdoctoral Science Foundation (No. 2018M642255)

REFERENCES

Choi, J. Y. (2005). Numerical study of base bleed projectile with external combustion. *AIAA 2005-4352*, 10-13.

Ding, Z., S. Chen and Y. Liu (2000). A study of wake flow field of base bleed. *Journal of Ballistics* 12(1), 43-47.

Ding, Z., S. Chen and Y. Liu (2002). Influence of ambient pressure on base bleed. *Journal of Ballistics* 14(1), 88-92.

Guo, X. (1994). *The exterior ballistics of base bleed projectile*. Beijing: National Defence Industry Press.

Kim, K. H. (1998). Accurate computation of hypersonic flows using AUSMPW+ scheme and shock-induced grid technique. *AIAA 98-2442*.

Luo, X., W. Yao, W. Xu, C. Zhuo, X. Wu and F. Feng (2015). Numerical investigation on the effect of combustion rate of propellant on the operation process and firing range of the base bleed projectile. *Chinese Journal of energetic materials* 23(11), 1111-1118.

Ma, L. and Y. Yu (2019). Numerical investigation of combustion and flow characteristics of combustion gas in rapid depressurization process of base bleed unit. *Acta armamentarii* 40(03), 488-499.

Mathur, T. and J. C. Dutton (1996). Base bleed experiments with a cylindrical afterbody in supersonic Flow. *Journal of Spacecraft and Rockets* 33(1), 30-37.

Menter, F. R. (1994). Two equation eddy viscosity turbulence models for engineering application, *AIAA Journal* 32(8), 1598-1605.

Ouyang, S., Z. Xie and C. Xu (2001). *High temperature air non-equilibrium flows*. Beijing: National Defence Industry Press.

Zhang, Z., L. Zhang and Z. Yin (2018). The effect of the initial propellant temperature on drag reduction characteristics of base bleed projectile. In *Procedings of 2018 International Conference on Defence Technology*, Beijing, China.

Zhang, Z. and L. Zhang (2017). Method of drag reduction and extend range based on variable burning rate of base bleed propellant. *Chinese Journal of Energetic Materials* 25(11), 925-931.

Zhuo, C., X. Wu and F. Feng (2014a). Numerical research on drag reduction of base bleed in supersonic flow. *Acta armamentarii* 35(1), 18-26.

Zhuo, C., X. Wu and F. Feng (2014b). Effect of base bleed type on drag reduction performance in supersonic flow. *Acta Aeronautica et Astronautica Sinica* 35 (8), 2144-2155.

Zhuo, C., W. Yao, X. Wu, W. Xu and F. Feng (2015). Research on operation process and firing range of base bleed projectile based on computational fluid dynamics coupled with particle trajectory. *Acta armamentarii* 36(11), 2062-2072.

Zhou, S. and Y. Yu (2020). Wake flow field characteristics of base-bleed projectiles with different nozzle structures under transient depressurization. *Acta armamentarii* 41(12), 2432-2443.

Zhou, L. (2002). *Multiphase turbulent reaction fluid dynamics*. Beijing: National Defence Industry Press.